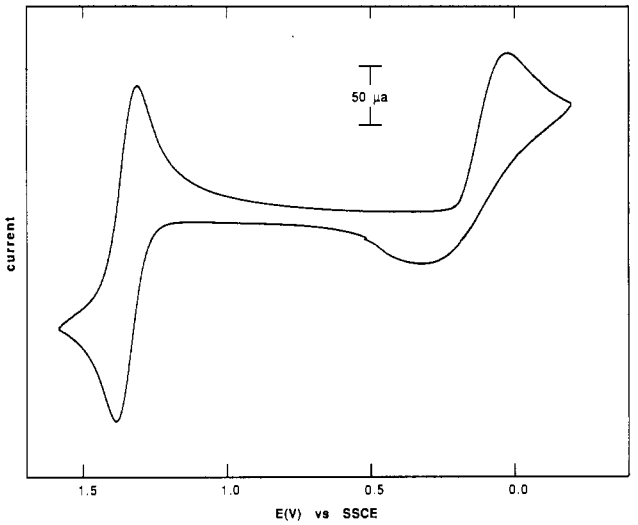

Figure 3. Cyclic voltammogram of **1** in CH_3CN with 0.100 M Et_4NClO_4 as supporting electrolyte, a Pt working electrode, a Pt-wire counter electrode, an SSCE reference electrode, and a scan speed of 50 mV/s.

a mononuclear Mn(IV) center. The EPR spectrum of a crude sample of **1** resembled that reported recently for a tris(thiohydroxamato)manganese(IV) complex,[7d] with signals in the g = 4 and g = 2 regions. However, after purification most of the absorption in the g = 2 region was removed. The resulting spectrum, shown in Figure 2, is similar to that reported for $[MnTPP(NCO)_2]$,[7g] except that hyperfine splitting in the g = 2 region was observed for the porphyrin complex. In contrast to the expectation that nearly octahedral coordination around Mn in **1** may give rise to a small axial zero-field splitting parameter (D), the data are consistent instead with a relatively large D value ($2D \gg h\nu \approx 0.31$ cm^{-1} at X-band frequencies).[15,16] The asymmetric appearance of the low-field signal and the fact that the crossing point of the same signal is at $g < 4$ (3.73) reveal a noticeable rhombic distortion. Despite the greater rhombicity in **1**, there is a distinct resemblance between its EPR spectrum in the low-field region and that of the g = 4.1 signal in PS II. This results supports the HAV model to the extent that it provides an example of a Mn(IV) species in a non-heme environment with a nearly axial EPR spectrum devoid of detectable ^{55}Mn nuclear hyperfine coupling in the g = 4 region.

The cyclic voltammogram of **1**, shown in Figure 3, reveals a quasi-reversible wave corresponding to the Mn^{IV}/Mn^{III} couple (1.35 V vs SSCE) and an irreversible III/II couple with $E_{p,c}$ = 0.02 V. To our knowledge compound **1** has the highest Mn^{IV}/Mn^{III} reduction potential among mononuclear complexes which have been isolated in their Mn^{IV} form. On the other hand, a higher IV/III couple has been reported for a complex isolated in the Mn^{II} form, $[Mn(terpyO_3)_2]^{2+}$ (1.77 V vs SCE).[17] Compound **1** may find use as a high-potential one-electron outer-sphere oxidizing agent. Complexes commonly used for this purpose include $Fe(cp)_2^+$ ($E_{1/2}$ = 0.307 V vs SCE)[18] and Ce^{4+} (1.20 V vs SCE).[19] Whereas the pyrazolylborate ligands in **1** destabilize Mn^{IV} with respect to Mn(III), alkoxide or deprotonated amide donors greatly stabilize the Mn(IV) level, as is illustrated by the low reduction potentials for $[Mn(salahp)_2]$ ($E_{p,c}$ = –0.32 V vs Ag/AgCl)[7a] and $[Mn(hps)_2]^{2+}$ ($E_{1/2}$ = –0.89 V vs SCE).[7o]

In conclusion, a novel Mn(IV) species with a nearly octahedral N_6 coordination environment has been isolated and characterized by X-ray crystallography, magnetic susceptibility, electrochemical, and spectroscopic measurements. Magnetic susceptibility and EPR data support the Mn(IV) formulation. In addition to contributing to the understanding of Mn(IV) species, **1** should find use as a high-potential oxidant. Finally, $[Mn(HB(3,5\text{-}Me_2pz)_3)_2]^{2+}$ may serve as a model for the Mn species that gives rise to the g = 4.1 signal in PS II.[20]

Acknowledgment. This work was supported by Grant No. GM382751-01 from the National Institute of General Medical Sciences. We thank Drs. Frederick J. Hollander and Marilyn M. Olmstead for assistance with the X-ray structure determinations. We are grateful to Professor K. Sauer and Dr. M. Klein, who kindly provided a preprint of ref 21.

Registry No. **1**, 122189-07-5; **2**, 122174-20-3.

Supplementary Material Available: For both **1** and **2**, fully labeled ORTEP drawings and tables of positional and isotropic thermal parameters, anisotropic thermal parameters, interatomic distances, and interatomic angles (25 pages). Ordering information is given on any current masthead page.

(15) Pedersen, E.; Toftlund, H. *Inorg. Chem.* **1974**, *13*, 1603–1612.
(16) Hempel, J. C.; Morgan, L. O.; Lewis, W. B. *Inorg. Chem.* **1970**, *9*, 2064–2072.
(17) Morrison, M. M.; Sawyer, D. T. *Inorg. Chem.* **1978**, *17*, 338–339.
(18) Bard, A. J.; Faulkner, L. R. *Electrochemical Methods*; Wiley: New York, 1980; p 701.
(19) Reference 18, p 699.
(20) A reviewer suggested that since it is generally thought that the environment around manganese in PS II consists of exclusively oxygen donors, compound **1** may have little relevance. However, this notion is usually based on spin-echo EPR results,[21] which apply *only* to the multiline site. No conclusions pertaining to the identity of ligands at the g = 4.1 center can be drawn from these observations. A recent report by Inoue et al.[22] suggests that histidine may be coordinated to manganese in PS II.
(21) Britt, R. D.; DeRose, V. J.; Chan, M. K.; Armstrong, W. H.; Sauer, K.; Klein, M. P. Submitted for publication.
(22) Tamura, N.; Ikeuchi, M.; Inoue, Y. *Biochim. Biophys. Acta* **1989**, *973*, 281–289.

Department of Chemistry
University of California
Berkeley, California 94720

Michael K. Chan
William H. Armstrong*

Received September 29, 1988

Aerobic and Anaerobic Photooxidation of *p*-Xylene in the Presence of Phosphotungstic Acid and Its Tetrabutylammonium Salt

Iso- and heteropolyoxoanions (POA) have been described as soluble analogues of transition-metal oxides, amenable to chemical tailoring and detailed characterization at a molecular level.[1-4] Recent interest in their chemistry has been fostered by their ability to mimic the interactions between organic substrates and catalytic oxide surfaces[5-8] and to promote the thermal or photochemical selective oxidation of these substrates.[9-11]

(1) Pope, M. T. *Heteropoly and Isopoly Oxometalates*; Springer-Verlag: Berlin, 1983.
(2) Pope, M. T. *Mixed-Valence Compounds*; Brown, D. B., Ed.; NATO ASI Series C58; D. Reidel Publ. Co.: Dordrecht, The Netherlands, 1980; p 365.
(3) Krebs, B. *Transition Metal Chemistry*; Mueller, A., Diemann, E., Eds.; Verlag Chemie: Weinheim, FRG, 1981; p 79.
(4) Day, V. W.; Klemperer, W. G. *Science* **1985**, *228*, 533.
(5) Prosser-McCartha, C. M.; Kadkhodayan, M.; Williamson, M. M.; Bouchard, D. A.; Hill, C. L. *J. Chem. Soc., Chem. Commun.* **1986**, 1747.
(6) Day, V. W.; Thompson, M. R.; Day, C. S.; Klemperer, W. G.; Liu, R. S. *J. Am. Chem. Soc.* **1980**, *102*, 5971.
(7) McCarron, E. M., III; Harlow, R. L. *J. Am. Chem. Soc.* **1983**, *105*, 6179.
(8) McCarron, E. M., III; Staley, R. H.; Sleight, A. W. *Inorg. Chem.* **1984**, *23*, 1043.
(9) Hill, C. L.; Bouchard, D. A. *J. Am. Chem. Soc.* **1985**, *107*, 5148.
(10) Fox, M. A.; Cardona, R.; Gaillard, E. *J. Am. Chem. Soc.* **1987**, *109*, 6347.
(11) Papacostantinou, E. *J. Chem. Soc., Chem. Commun.* **1982**, 12.

0020-1669/89/1328-3779$01.50/0 © 1989 American Chemical Society

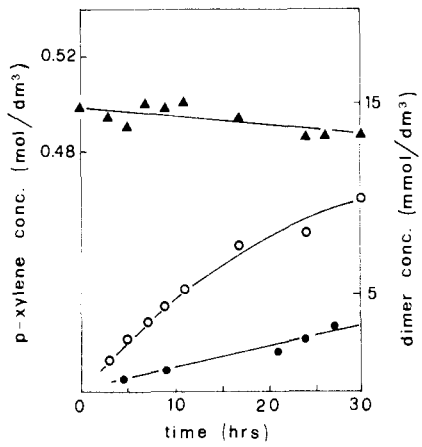

Figure 1. Anaerobic catalytic photoreaction of *p*-xylene with **2** shown by plots of decrease in *p*-xylene (▲) and production of 1,2-di-*p*-tolylethane (●, ○) The corresponding open and filled symbols indicate the absence (●) or the presence (○) of PtO_2 as cocatalyst.

During the last 3 years the ability of POA's to act as oxidation catalysts, well-known for alcohols and related molecules,[12-15] has been extended to other, more oxidation-resistant organics,[16-18] and the limits of their catalytic capabilities are still unknown.

We now report that a novel substrate, namely alkylbenzenes, can be photooxidized, both in an inert atmosphere or under oxygen, by using $H_3PW_{12}O_{40}(H_2O)_n$ (**1**) or its salt $(Bu_4N)_3PW_{12}O_{40}$ (**2**) as an oxidation catalyst. With the aim of exploring the feasibility of the above reactions, we used mild reaction conditions[19] and chose *p*-xylene as a test compound because of its central position in the scale of oxidizability of organic compounds.[20]

Figure 1 summarizes the essential results of the anaerobic reaction carred out by using a substrate/catalyst ratio of 250/1. In the presence of **1** or **2** and an equimolar amount of PtO_2, as hydrogen evolution cocatalyst, ca. 4% of *p*-xylene is selectively converted to 1,2-di-*p*-tolylethane, after 30 h of irradiation, whereas no reaction is observed in the absence of the POA catalyst:

$$PW_{12}O_{40}^{3-} + h\nu \rightarrow PW_{12}O_{40}^{3-*} \quad (1)$$

$$PW_{12}O_{40}^{3-*} + 2MePhMe \rightarrow PW_{12}O_{40}^{red} + MePhCH_2CH_2PhMe + 2H^+ \quad (2)$$

$$PW_{12}O_{40}^{red} + 2H^+ \rightarrow PW_{12}O_{40}^{3-} + H_2 \quad (3)$$

According to the above reaction scheme, the dimer is formed via coupling of two benzyl radicals resulting from deprotonation of two aromatic cation radicals.

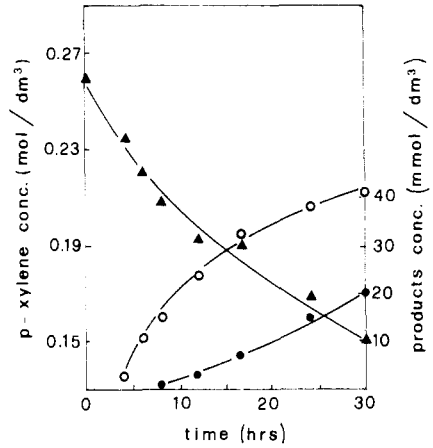

Figure 2. Aerobic catalytic photoreaction of *p*-xylene with **1** shown by plots of decrease in *p*-xylene (▲) and production of *p*-tolualdehyde (○) and *p*-toluic acid (●).

The conversion rate of *p*-xylene is essentially the same observed by Yamase in the case of olefins,[16] but the selectivity is higher since no trimers or higher oligomers were detected. This may be ascribed to both the high termination rate of the *p*-xylene radicals and to their higher stability compared with alkyl radicals.[20] Reaction with the CH_3CN solvent and traces of water to produce *p*-tolylacetamide (as correspondingly found when the substrates are alkanes[17a]) is not competitive with the dimerization process and was not observed. In addition we note that concentrated solutions of **1** or **2** and *p*-xylene are bright yellow, suggesting formation of a POA–substrate charge-transfer complex, which appears to be a necessary prerequisite for the following oxidation of the substrate.[10] Therefore high radical concentration in the vicinity of the catalyst molecules further accounts for the selective dimerization of *p*-xylene.

The rate-determining step of the cycle shown in (1)–(3) appears to be the reoxidation of $PW_{12}O_{40}^{red}$. In fact, if addition of PtO_2, which enables H_2 to be evolved at a less negative reduction potential, is omitted, the amount of 1,2-di-*p*-tolylethane produced in 24 h is nearly equal to the initial concentration of POA. Under the assumption that the final steady-state of the POA catalyst is the 2e-reduced product,[21] the process turns out to be essentially stoichiometric. Further, the drop of ca. 50% in the efficiency of the Pt cocatalyst after about 26 h of photolysis[22] may explain the deviation from linearity of dimer formation.

As opposed to the above results, large *p*-xylene conversion (almost 40% after 30 h irradiation) is obtained if the reaction is run under a slight overpressure of oxygen.

Figure 2 shows that *p*-tolualdehyde is the main product and then partially converts, as expected, to *p*-toluic acid, the presence of POA being not required in this last step.

$$PW_{12}O_{40}^{3-*} + MePhMe \rightarrow PW_{12}O_{40}^{red} + MePhCHO + MePhCH_2OH + MePhCOOH \quad (4)$$

$$PW_{12}O_{40}^{red} + \tfrac{1}{2}O_2 + 2H^+ \rightarrow PW_{12}O_{40}^{3-} + H_2O \quad (5)$$

The total yield of aldehyde and acid is about 25% (respectively 17% and 8%) of the initial substrate concentration, and corresponds to ca. 60 turnovers. In addition, GC/MS showed the presence, in low percentages, of the corresponding alcohol as well as terephthalic acid (see below). The remaining amount of reacted *p*-xylene (less than 10% of the initial concentration) is accounted for by oligomeric oxygenated byproducts.

The importance of the POA catalyst is more evident when a strong radical scavenger as O_2 is present. Benzyl radicals, very likely formed at the surface of the POA^{red} molecules, are trapped by O_2 to form arylperoxy radicals $ArCH_2O_2$, giving rise to a classical autooxidation mechanism. The corresponding aldehyde

(12) Yamase, T.; Takabayashi, N.; Kaji, M. *J. Chem. Soc., Dalton Trans.* **1984**, 793.
(13) Akid, R.; Darwent, J. R. *J. Chem. Soc., Dalton Trans.* **1985**, 395.
(14) Nomiya, K.; Maeda, K.; Miyazaki, T.; Miwa, M. *J. Chem. Soc., Dalton Trans.* **1987**, 961.
(15) Darwent, J. R. *J. Chem. Soc., Chem. Commun.* **1982**, 798.
(16) Yamase, T.; Usami, T. *J. Chem. Soc., Dalton Trans.* **1988**, 183.
(17) (a) Renneke, R. F.; Hill, C. L. *J. Am. Chem. Soc.* **1986**, *108*, 3528. (b) Renneke, R. F.; Hill, C. L. *J. Am. Chem. Soc.* **1988**, *110*, 5461.
(18) Renneke, R. F.; Hill, C. L. *Nouv. J. Chim.* **1987**, *11*, 713.
(19) A 125-W mercury lamp, in conjunction with a cold-water Pyrex cutoff filter was used as light source of irradiation. Commercial *p*-xylene (purity > 99.0%) and $H_3PW_{12}O_{40}(H_2O)_n$ ($n \approx 18$ by TGA) were employed. $(TBA)_3PW_{12}O_{40}$ was prepared by reaction of **1** and Bu_4NBr and crystallized from acetonitrile. Acetonitrile was distilled from CaH_2 under a stream of purified N_2. Anaerobic reactions were performed by dissolving *p*-xylene (5×10^{-1} mol·dm^{-3}) and **1** or **2** (2×10^{-3} mol·dm^{-3}) in CH_3CN (175 mL), eventually adding PtO_2 (2×10^{-3} mol·dm^{-3}) as the H_2 evolution catalyst. During the irradiation, the deaerated Pyrex flask was kept under a slight, constant overpressure of N_2, and the reaction was stirred throughly at 25 °C. Alternatively, aerobic reactions were performed without the PtO_2 and under a slight overpressure of O_2. Product identification was accomplished by direct analysis of the photolysate by GC and co-injection of authentic samples. After a standard workup, isolable products were identified by IR, NMR, and GC-MS methods. Blank test reactions were carried out in the absence of the POA catalyst.
(20) Sheldon, R. A.; Kochi, J. K. *Metal-Catalyzed Oxidations of Organic Compounds*; Academic Press Inc.: New York, 1981; Chapter 10.
(21) Low-temperature EPR spectroscopy failed to show any significant concentration of the paramagnetic 1e-reduced catalyst.
(22) Ioannidis, A.; Papacostantinou, E. *Inorg. Chem.* **1985**, *24*, 439.

can then be formed either by redox reaction of the $ArCH_2O_2$ with the POA^{red} catalyst, or, due to the high termination rate of the arylperoxy radicals, by disproportionation of two $ArCH_2O_2$. In this case the corresponding alcohol is also formed.[20] Subsequent oxidation of the latter may also give *p*-tolualdehyde. In turn, oxidation of the aldehyde produces the corresponding carboxylic acid. At this point, reoxidation of the reduced POA catalyst in the presence of excess oxygen is an easy and fast process, which efficiently closes the catalytic cycle.[11]

Further, we note that, after about 20 h of irradiation, the reaction performed either with **1** or **2** showed the presence of a white precipitate (ca. 3% of the starting *p*-xylene) that turned out to be analytically pure terephthalic acid. At this point, light scattering and diffusion from the heterogeneous reaction mixture considerably decreases the photocatalytic reaction rate. However, it is noteworthy that, after the first oxidation step, deactivation of the second CH_3 by the electron-withdrawing carboxylic group does not prevent complete oxidation of *p*-xylene.

Finally, we point out that recovery of the catalyst, after both the anaerobic and the aerobic reactions, gives partially insoluble products that, although retaining the intact POA structure (IR spectroscopy), contain small amounts of organics strongly bound to the inorganic acid.[23]

Investigation of this and other aspects of the reported processes are under way and will be reported at a later stage.

(23) Preliminary results (^1H NMR) indicate that traces of CH_3CN oxidation products are present.

Istituto di Teoria e Struttura Elettronica e Comportamento Spettrochimico dei Composti di Coordinazione del CNR
P.O. Box 10
00016 Monterotondo Stazione, Roma, Italy

Donato Attanasio*
Lorenza Suber

Received April 17, 1989

Kinetics and Mechanism of Electron Transfer from Pentacarbonylrhenate to Metal Carbonyl Dimers by Infrared Stopped-Flow Spectroscopy

Single-electron transfer is a reaction of importance in organic synthesis, homogeneous catalysis, and organometallic chemistry.[1-3] Reactions of metal carbonylates with dimers involve electron transfer and offer the opportunity to study single-electron transfer between organometallic complexes.[4] These reactions occur rapidly, and we have developed an infrared stopped-flow system to examine such reactions. In this communication we report on the reactions of $Re(CO)_5^-$ with the dimers $Mn_2(CO)_{10}$, $Co_2(CO)_8$, and $Cp_2Mo_2(CO)_6$.

Product determination of reactions 1–3 was examined by infrared spectroscopy. Spectral data are given in Table I. All

$$2Re(CO)_5^- + Mn_2(CO)_{10} \rightarrow Re_2(CO)_{10} + 2Mn(CO)_5^- \quad (1)$$

$$2Re(CO)_5^- + Co_2(CO)_8 \rightarrow Re_2(CO)_{10} + 2Co(CO)_4^- \quad (2)$$

$$2Re(CO)_5^- + Cp_2Mo_2(CO)_6 \rightarrow Re_2(CO)_{10} + 2CpMo(CO)_3^- \quad (3)$$

(1) Eberson, L. *Electron Transfer Reactions in Organic Chemistry*; Springer-Verlag: Berlin, 1987.
(2) Kochi, J. K. *Free Radicals*; Wiley-Interscience: New York, 1973.
(3) Stiegman, A. E.; Tyler, D. R. *Comments Inorg. Chem.* **1986**, *5*, 215.
(4) Dessy, R. E.; Weissman, P. M. *J. Am. Chem. Soc.* **1966**, *88*, 5129.

Table I. Infrared Spectral Data for the Anions and Dimers

$Mn_2(CO)_{10}$	2050 (m)	2015 (s)	1985 (w)	
$Co_2(CO)_8$	2070 (m)	2040 (m)	1950 (m)	1885 (w)
	1840 (m)			
$Cp_2Mo_2(CO)_6$	1950 (m)	1910 (m)	1775 (w)	1720 (w)
$Re_2(CO)_{10}$	2070 (s)	2010 (m)	1965 (m)	
$(PPN)Re(CO)_5$	1906 (m)	1860 (s)		
$(PPN)Mn(CO)_5$	1890 (m)	1860 (s)		
$(PPN)CpMo(CO)_3$	1893 (s)	1780 (s)		
$(PPN)Co(CO)_4$	1890 (m)			

Table II. Observed Rate Constants for Reaction of $Re(CO)_5^-$ with M_2

M_2	$[M_2]$,[a] M	k_{obsd},[b] s^{-1}
$Cp_2Mo_2(CO)_6$	2.0×10^{-3}	$1.04 \times 10^{-1} \pm 1.5 \times 10^{-3}$
	2.00×10^{-2}	$5.31 \times 10^{-1} \pm 1.2 \times 10^{-3}$
	6.00×10^{-2}	$1.12 \pm 3.6 \times 10^{-2}$
	8.00×10^{-2}	$1.78 \pm 2.0 \times 10^{-2}$
	2.00×10^{-1}	$4.08 \pm 5.7 \times 10^{-2}$
$Mn_2(CO)_{10}$	1.00×10^{-3}	$4.44 \times 10^{-2} \pm 3.3 \times 10^{-4}$
	2.00×10^{-2}	$5.04 \times 10^{-2} \pm 3.4 \times 10^{-4}$
	6.00×10^{-2}	$9.31 \times 10^{-2} \pm 3.3 \times 10^{-3}$
	8.00×10^{-2}	$1.39 \times 10^{-1} \pm 2.5 \times 10^{-3}$
	2.00×10^{-1}	$3.01 \times 10^{-1} \pm 1.9 \times 10^{-3}$
$Co_2(CO)_8$	3.0×10^{-2}	2.07 ± 0.04
	6.00×10^{-2}	2.60 ± 0.01
	8.00×10^{-2}	2.70 ± 0.02
	1.00×10^{-1}	3.00 ± 0.02

[a] Concentrations are in molarity, $[Re(CO)_5^-] = 1.00 \times 10^{-3}$ M. [b] k_{obs} values were calculated using the OLIS 4120AT computer program. The standard deviations are reported.

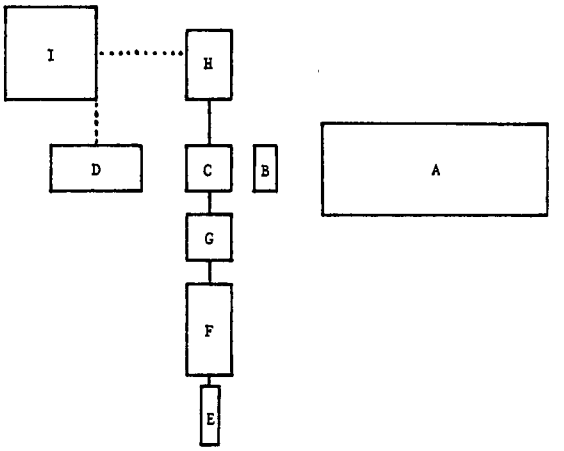

Figure 1. Schematic of the infrared stopped-flow spectrophotometer. A is a tunable CO laser (Edinburgh Instruments PL 3), B is an iris diaphragm, C is an Irtran-2 flow-through cell (Wilmad Glass Co., Inc.), D is a HgCdTe detector (Infrared Associates, Inc.), E is an air cylinder (Power Drive, Inc.), F is the syringe assembly, G is the Berger ball mixer (Research Instruments and Mfg. and Commonwealth Technology, Inc.), H is the stopping syringe assembly, and I is the stopped-flow operating system (OLIS). The dashed lines indicate an electrical connection.

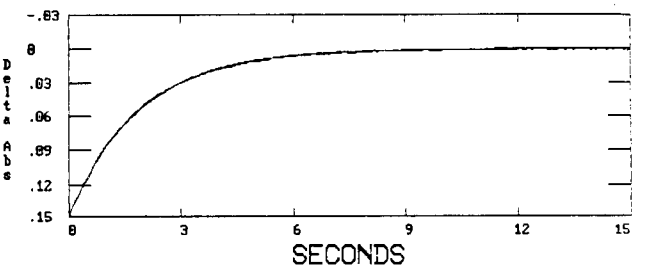

Figure 2. Plot of the kinetic data and fit for the reaction of $Re(CO)_5^-$ (1×10^{-3} M) with $Cp_2Mo_2(CO)_6$ (2×10^{-2} M) following the loss of $Re(CO)_5^-$ at 1860 cm^{-1}.

reactions were run in THF, the THF was removed, and the solid was extracted with hexanes to separate the dimeric species from the anions. Reactions 1–3 were quantitative; the reverse reactions

0020-1669/89/1328-3781$01.50/0 © 1989 American Chemical Society